Carbon-Nanotube-Supported Copper Polyphthalocyanine for Efficient and Selective Electrocatalytic CO 2 Reduction to CO

Dilan Karapinar, Andrea Zitolo, Tran Ngoc Huan, Sandrine Zanna, Dario Taverna, Luiz Henrique Galvao Tizei, Domitille Giaume, Philippe Marcus, Victor Mougel, Marc Fontecave

Carbon Nanotube supported Copper Polyphthalocyanine for Efficient and Selective Electrocatalytic CO_2 Reduction to CO

Dilan Karapinar, [1] *Andrea Zitolo,*[2] *Ngoc Tran Huan,*[1] *Sandrine Zanna,*[3] *Dario Taverna,*[4] *Luiz Henrique Galvão Tizei,*[5] *Domitille Giaume,*[3] *Philippe Marcus,*[3] *Victor Mougel,*[1ǂ*] *Marc Fontecave*[1*]

[1]Laboratoire de Chimie des Processus Biologiques, UMR CNRS 8229, Collège de France-CNRS-Sorbonne Université, PSL Research University, 11 Place Marcelin Berthelot, 75005 Paris, France.

[2] Synchrotron SOLEIL, L'Orme des Merisiers Saint-Aubin - BP 48, 91192 Gif-sur-Yvette, France.

[3] Chimie Paris Tech, PSL Research University, CNRS, Institut de Recherche de Chimie de Paris, 11 rue Pierre et Marie Curie, 75005 Paris, France

[4] Institut de Minéralogie, de Physique des Matériaux et de Cosmochimie, UMR 7590 Sorbonne Universités, CNRS, Museum National d'Histoire Naturelle, IRD, 4 place Jussieu, 75005 Paris, France.

[5] Laboratoire de Physique des Solides, Université Paris Sud, Bât 510, 91405 Orsay, France.

ǂ V. Mougel current address : Department of Chemistry and Applied Biosciences, Eidgenössische Technische Hochschule Zürich, 8093 Zurich, Switzerland.

* to whom correspondence should be addressed : marc.fontecave@college-de-france.fr; mougel@inorg.chem.ethz.ch

KEYWORDS. CO_2 reduction – electrocatalysis – copper – polyphthalocyanine -carbon nano supports.

Abstract

Electroreduction of carbon dioxide (CO_2RR) into CO is one of the simplest ways to valorize CO_2 as a source of carbon. Here we report an original, cheap and robust, Cu-based hybrid catalytic material, consisting of a polymer of Cu phtalocyanine coated on carbon nanotubes (CNTs), which proved selective for CO production (Faradic yield 80%) at relatively low overpotentials. Polymerisation of Cu phtalocyanine here is shown to have a drastic effect on the selectivity of the reaction since molecular Cu phtalocyanine is instead selective for proton reduction under the same conditions. Finally, while the material only displays isolated Cu sites, within a phtalocyanine-like CuN_4 coordination, *in situ* and *operando* X-ray absorption spectroscopy show that the Cu atoms fully convert, under operating conditions, into Cu nanoparticles, which are likely to be the catalytic species. Interestingly this restructuration of the metal sites is reversible.

Introduction

Electroreduction of carbon dioxide (CO_2RR) into carbon monoxide is one of the simplest ways to valorize CO_2 as a source of carbon, since CO is an energy-rich and reactive substrate for a number of reactions in the chemical industry[1]. This reaction is endergonic and involves the transfer of two electrons and two protons and thus requires catalysts to overcome the associated kinetic barrier. These kinetic and thermodynamic challenges often also translate into a selectivity challenge since the kinetically and thermodynamically easier proton reduction to hydrogen can also occur, competing with CO_2 reduction. Efficient and selective catalysts are hence needed to envision a large scale electrocatalytic conversion of CO_2 into CO.

Among molecular catalysts proposed for CO_2 reduction to CO, metal porphyrins and metal phtalocyanines have been extensively studied during the last 20 years due to their high CO_2RR selectivity, even though they still suffer from low current densities, large overpotentials and low stability[1-2]. Heterogenization is an appealing strategy to improve their performances while preserving their high selectivity and generating solid electrodes ready to be implemented in practical technological devices (electrolyzers). A widely used method consists in anchoring metal porphyrins and metal phtalocyanines on carbon nanotubes (CNTs), via covalent grafting or non covalent interactions[3]. Alternatively the metal complexes can be used as building blocks of the material itself, for example in the form of covalent organic frameworks[4]. Very recently, such an approach was combined with high-surface area conductive supports, for example through the *in situ* polymerisation of metal phtalocyanines on conductive carbon scaffolds such as carbon nanotubes[5]. The resulting hybrid material, in which a thin polymer coating layer is deposited at the surface of the CNTs, displays a number of potential advantages: (i) its synthesis is carried out at relatively mild conditions; (ii) within a polymer form, a much higher robustness of the catalyst can be achieved; (iii) electron transfer from the highly conductive support and the polymer layer is facilitated; (iv) a quite large density of active metal sites can be obtained. So far this strategy has been underexplored in the context of the search for novel molecular-based heterogeneous catalysts for CO_2 reduction. To our knowledge, the only example of such a polymer catalyst is the recently reported cobalt polyphtalocyanine-CNT hybrid electrocatalyst, which allows electroreduction of CO_2 into CO with large faradic efficiency (>90%) and turnover frequency combined with excellent stability[5]. Considering recent reports showing the potential of Cu-

porphyrins and crystalline Cu-phtalocyanine as catalysts for the electroreduction of CO_2 into a variety of products[2g, 2i], we were intrigued by the possibility to elaborate a copper polyphtalocyanine material and evaluate its catalytic properties.

Here we thus describe a novel material, a copper polyphtalocyanine-CNT (CNT = Carbon NanoTubes) hybrid material, which has been structurally characterized. It displays an excellent catalytic activity for CO_2 electroreduction to CO with a high FY of almost 80% at relatively low overpotentials. Such a high selectivity for CO is unique for a Cu-based material. Furthermore, this is a very interesting case of a drastic positive effect of polymerization, since monomolecular Cu phtalocyanine, deposited on CNTs, was shown to be a relatively poor catalyst for CO_2 electroreduction, generating H_2 as the only product at such potentials under the same conditions. Finally, utilizing *operando* X-ray absorption spectroscopy (XAS) we find that the Cu atoms convert into Cu nanoparticles under operating conditions, suggesting the latter to be the actual catalytically active species. Interestingly this restructuration of the metal sites is fully reversible since, upon reoxidation, the Cu nanoparticles disappear and the isolated Cu-phtalocyanine-like sites are reconstituted. This finding raises the general question of the nature of the catalytically active species in the case of this class of metal polyphtalocyanine catalysts, an issue not previously addressed.

RESULTS AND DISCUSSION

Synthesis and characterization of the CuPolyPc@CNT

CuPolyPc@CNT was prepared by heating 1,2,4,5-tetracyanobenzene (TCNB) together with cuprous chloride ($CuCl_2$) under Ar atmosphere on pre-oxidized multi-walled carbon nanotubes (CNT) templates dispersed in ethylene glycol during 2.5 hours (see Experimental Procedures for details) following comparable synthetic routes used for Fe[6] , Cu[7] and Co[5] polyphthalocyanine (scheme 1). The product was washed then with H_2SO_4 (8 M) aqueous solution, acetone, ethanol and dried under vacuum for 12h. The relative amounts of the starting precursors were chosen to achieve Cu to CNT weight ratio of about 1.5% in the final product. Inductively Coupled Plasma – Atomic Emission Spectroscopy (ICP-AES) analysis showed that the actual Cu to CNT weight ratio was about 1.2%.

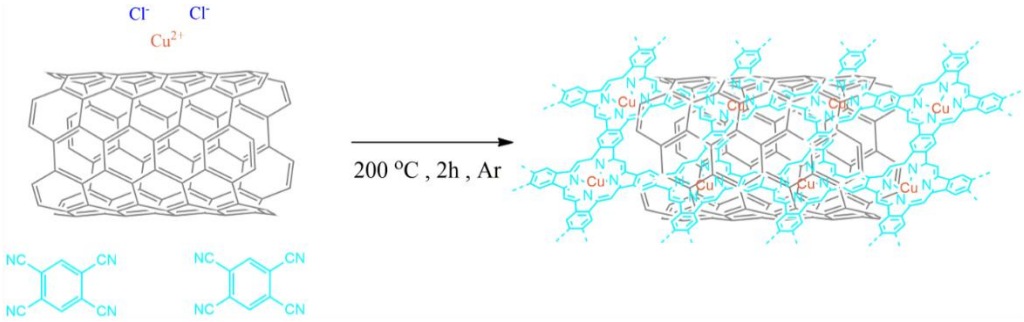

Scheme 1: Synthesis of CuPolyPc@CNT

The material was analyzed by various electron microscopy techniques. Scanning electron microscopy (SEM) (Figure S1) and Transmission electron microscopy (TEM) (Figure S2) images showed that the carbon nanotubes were coated with polymer and that the hybrid material retained the one-dimensional fiber-like morphology. Atomic-resolution high-angle annular dark-field scanning transmission electron microscopy (HAADF-STEM) images of CuPolyPc@CNT (Figure 1) showed the presence of multiple bright dots which likely correspond to the presence of isolated Cu atoms.

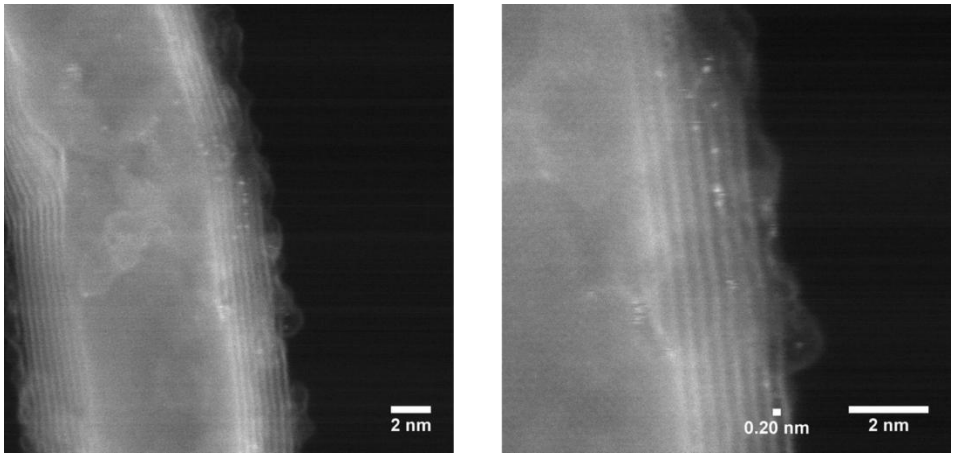

Figure 1: HAADF-STEM images of CuPolyPc@CNT

X-ray photoelectron spectroscopy (XPS) analysis of CuPolyPC@CNT was carried out after deposition on a Gas Diffusion layer (GDL) (see below). It showed Cu $2p_{3/2}$ peaks at 932.5 and 935.0 eV indicating that Cu is predominantly in the Cu^{2+} oxidation state (Figure S3). The analysis of the N 1s region revealed the presence of pyridinic (398.6 eV), pyrrolic (401.0 eV), and N-Cu

signals (399.7 eV), analogous to what is typically observed with metal polyphthalocyanine hybrid materials[6b].

Finally, the electrochemical active surface area (ECSA) of the electrode consisting of CuPolyPc@CNT deposited on a GDL was shown to be 1.73 cm^2 per 1 cm^2 geometric surface area, based on standard methods (Figure S4).

Electrocatalytic CO_2RR activity of CuPolyPc@CNT

For the electrochemical characterization of the catalytic properties of CuPolyPc@CNT, electrodes were prepared in three steps. An ink was first obtained by dispersing 2 mg of CuPolyPc@CNT in a Nafion® suspension in isopropanol, and then deposited on GDL followed by a final drying step as described in the Experimental section.

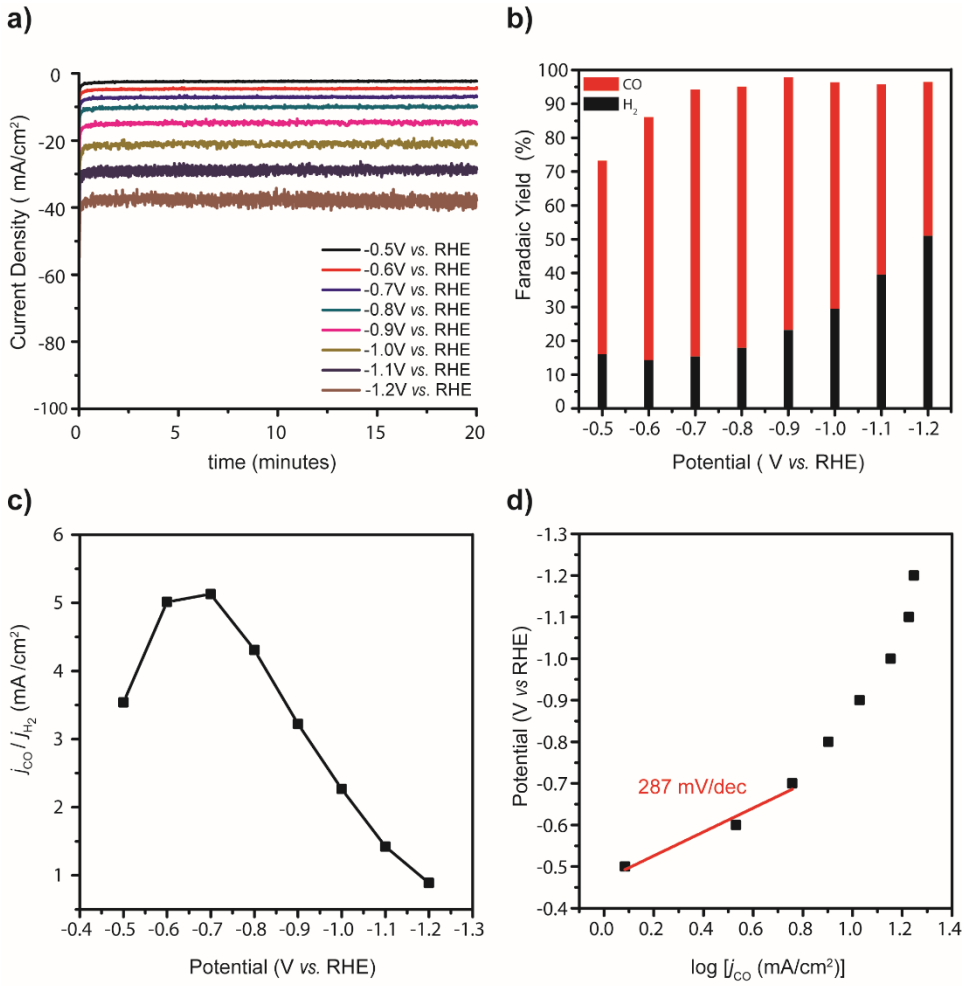

Figure 2. (a) Total current density during electrolysis at various applied potentials and **(b)** Faradaic yields for CO and H_2 after 20 min electrolysis**; (c)** Partial current densities of CO production over H_2 production after 20 min electrolysis; **(d)** Tafel plot for CO production was determined between - 0.5 and -1.2 V, with the regression coefficient R^2 = 0.931. All CPE experiments were run in a 0.1 M $CsHCO_3$ aqueous solution under 10 mL/min flow of CO_2.

Electrocatalytic CO_2 reduction was first investigated by linear sweep voltammetry (LSV) in CO_2–saturated 0.1 M $CsHCO_3$ in the 0.0 to –1.2 V *vs.* RHE potential range of (Figure S5). Cs^+ cations in the electrolyte were chosen based on their known ability to impede the H_2 evolution reaction and favour CO_2 reduction vs proton reduction.[8] The LSV shows a catalytic wave with an onset potential at about –0.45 V *vs.* RHE, namely with an overpotential of 340 mV, considering that the main product of the reaction is CO (see below).

To get insight into the selectivity of the catalyst, controlled-potential electrolysis (CPE) has been conducted at potential values between –0.5 to –1.2 V (all potentials are indicated *vs.* RHE) in a 0.1 M $CsHCO_3$ aqueous solution under a constant flow of gaseous CO_2 (10 mL/min) within the electrolyte. During the 20 minutes of electrolysis at all potentials the current remained constant (Figure 2a), after which the liquid and gaseous reaction products were analyzed, as described in the experimental section. In all cases, only CO and H_2 could be observed in the gas phase and no evidence for the presence of other gaseous products such as methane and hydrocarbon could be obtained. In addition, no liquid product, formic acid and alcohols, could be detected by ^1H nuclear magnetic resonance spectroscopy analysis of the solution.

The selectivity of the reaction was potential-dependent. The highest faradic yield (FY) for CO (80 %) was obtained at –0.7 V *vs.* RHE with a stable average current density of > 7 mA/cm^2 (Figure 2a and Figure 2b). The selectivity for CO formation relative to hydrogen evolution could be better visualized by plotting the ratio of the partial current density (j_{CO}) for CO production over the partial current density (j_{H2}) for H_2 production (Figure 2c). Absolute values of j_{CO} and j_{H2} are reported in Figure S6. Figure 2c clearly shows that at more cathodic applied potentials than –0.7 V *vs.* RHE, the j_{CO}/ j_{H2} ratio greatly decreases, from the highest value of about 5, resulting in lower FY for CO (Figure 2b).

A Tafel plot derived from partial current densities for CO production as a function of over-potentials (Figure 2d) showed that CuPolyPc@CNT exhibits the lowest Tafel slope value (~287

mV/dec) between –0.4 and –0.8 V applied potential. This suggests that the rate-determining step is likely to be the initial electron transfer to CO_2 to form a CO_2^- intermediate.

The combination of CuPolyPc with CNT proved essential, as shown by the following control experiments. Indeed when molecular Cu phthalocyanine, in place of CuPolyPc, was deposited on CNT, with a similar amount of loaded Cu, the resulting catalyst was much less efficient, with lower current density at –0.7 V and – 0.8 V *vs.* RHE (Figure S7). Furthermore, it did not show any CO_2RR activity, the only observed product being H_2 with no detectable trace of CO. Finally, when carbon nanofibers (CNF) were used, in place of CNTs, as the conductive carbon support for CuPolyPc, a much less efficient catalyst was obtained, displaying lower current density and much lower FY for CO production (Figure S8). Unfortunately we were unable to correctly achieve the polymerization directly on a carbon paper (GDL), so that the control CuPolyPc/GDL material (thus in the absence of CNT) could not be studied. The greater activity and selectivity of CuPolyPc@CNT might originate from a combination of factors: higher surface area and higher electrical conductivity of CNTs as well as a more favorable interface between the transient active Cu nanoparticles, the polymeric ligand and the CNT support.

In addition, CuPolyPc@CNT was shown to be a very stable catalyst. As shown in Figure 3, it can operate during 50 hours electrolysis at –0.7 V *vs.* RHE, with no decay of the FY for CO production (average value of 80%) and an average current density value of 7.5 mA/cm^2. The catholyte solution was shown, by ICP-MS analysis, to contain after electrolysis less than 0.01% of the total Cu load, thus excluding dissolution of the material during operation.

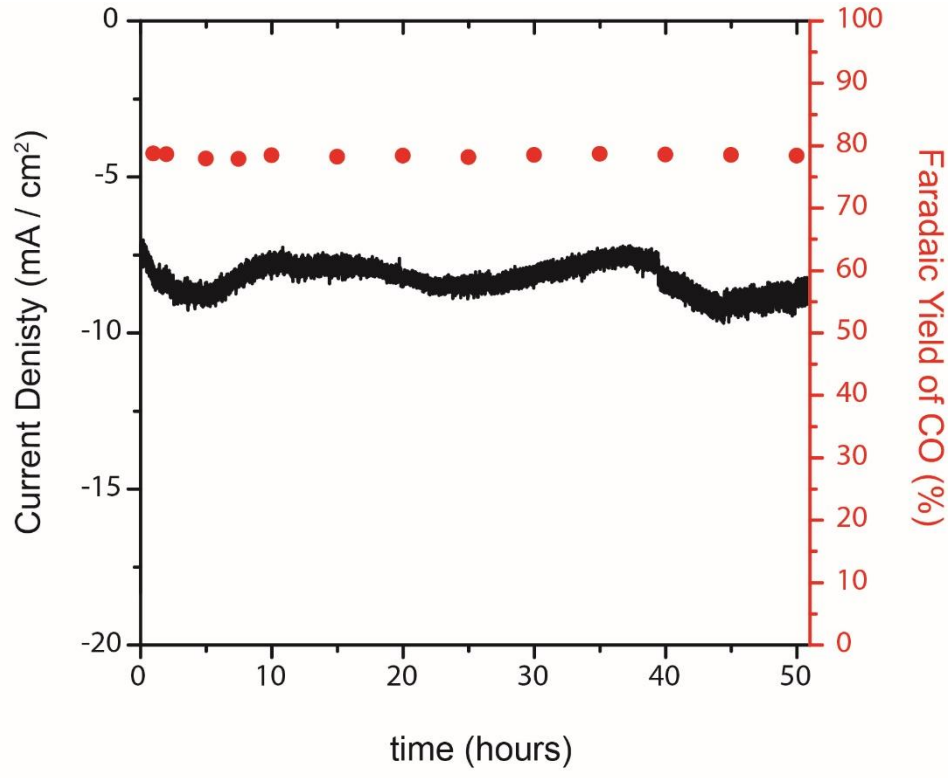

Figure 3. Current density and Faradaic yield for CO production as a function of time during CPE. Electrolysis was run at a constant potential of –0.7 V *vs.* RHE, using the CuPolyPc@CNT electrode in a 0.1 M $CsHCO_3$ aqueous solution under a flow of CO_2 (10 mL/min).

Post-electrolysis and *operando* characterization of the material

SEM analysis of the electrode after electrolysis showed that the CNTs were still present on its surface (Figure S1c). *Ex-situ* characterization of CuPolyPc@CNT immediately after electrolysis by cyclic voltammetry (Figure S9) revealed a new anodic signal (peak 1) at 0.08 V *vs.* Ag/AgCl and a new cathodic peak (peak 2) at around –0.06 V *vs.* Ag/AgCl, consistent with the presence of metallic Cu nanoparticles deposited on the surface of the material. This was consistent with XPS data, demonstrating the absence of Cu^{2+} species in the Cu $2p_{3/2}$ region (Figure S10) and with the XANES data showing that Cu was mainly in the Cu^0 state (see below).

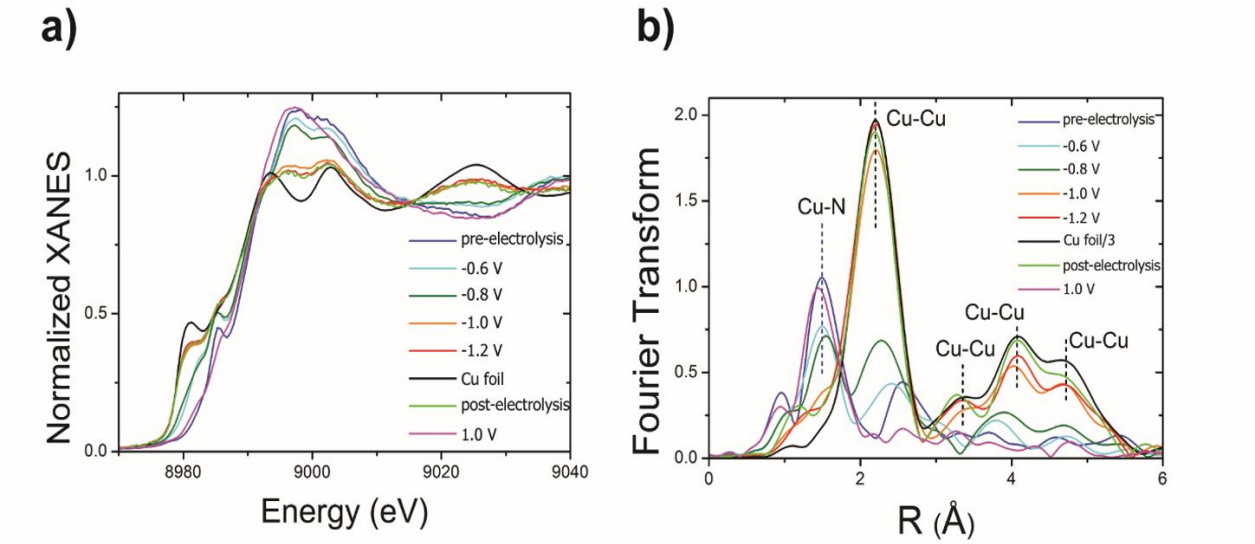

Figure 4. ***Operando*** **XAS characterization of CuPolyPc@CNT at the Cu-K edge. (a)** K-edge XANES spectra of CuPolyPc@CNT under no potential applied (blue line) , during electrolysis at –0.6 V *vs.* RHE (light blue line) , at –0.8 V *vs.* RHE (green line) , at –1.0 V *vs.* RHE (orange line), at –1.2 V *vs*. RHE (red line) and metallic copper (black line), after electrolysis under no potential applied (light green line) and at 1.0 V *vs.* RHE (pink line); **(b)** Fourier transform of the experimental EXAFS spectra of CuPolyPc@CNT under no potential applied (blue line) , during electrolysis at *vs.* (light blue line) , at –0.8 V *vs.* RHE (green line) , at –1.0 V *vs.* RHE (orange line), at –1.2 V *vs.* RHE (red line) and metallic copper (black line), after electrolysis under no potential applied (light green line) and at 1.0 V *vs.* RHE (pink line). All CPE experiments were run in a 0.1 M CsHCO3 aqueous solution for 20 minutes.

Recent studies of molecular Cu-phthalocyanine and its analysis during CO_2 electrolysis by *operando* spectroscopic techniques revealed the transient formation of very small metallic Cu nanoparticles, likely active as catalysts. This restructuration of the metal sites was also shown to be reversible[2j]. In order to investigate whether CuPolyPc@CNT enjoys the same restructuration of Cu sites, we resorted to *operando* XAS techniques under electrolysis in the presence of CO_2. As shown in Figure 4a, the X-ray absorption near edge structure (XANES) spectra at the copper K-edge of the material under electrocatalytic conditions revealed a shift in the edge position from 8983.93eV to 8979.2 eV for applied potentials more cathodic than –0.6 V *vs.* RHE, indicative of a change of the Cu oxidation state from +II to 0 (the metallic copper K-edge energy position is indeed 8979 eV, see Figure 4a). Just after electrolysis, all Cu atoms were in the Cu(0) state. The Extended X-ray Absorption Fine Structure (EXAFS) spectra of CuPolyPc@CNT were also very informative (Figure 4b and Figure S11). While only Cu-N features, typical for single site CuN_4 coordination present in Cu phtalocyanine, could be observed at about 1.5 Å before electrolysis,

thus excluding the presence of Cu nanoparticles, the characteristic peaks associated with a Cu-Cu backscattering appeared at about ~2.2 Å and between 3 and 5 Å, under operating conditions at potentials more negative than –0.6 V *vs.* RHE. These peaks provided a clear evidence for the formation of metallic copper nanoparticles (CuNP) under electrocatalytic conditions. While a mixture of CuN_4 sites and CuNP was present at potentials down to –0.8 V, Cu was almost exclusively in the form of CuNP at potentials more negative than –1.0 V. After electrolysis at –1.2 V *vs.* RHE, indeed, and in agreement with the XANES data, no CuN_4 site could be observed. As a further confirmation, we performed an EXAFS fit of CuPolyPc@CNT at -1.2V: the EXAFS calculations confirmed the well-known metal Cu face-centered cubic crystal structure, with lower coordination numbers due to the nanoparticle nature of the active phase (Figure S12 and Table S1).

Interestingly, this restructuration of the Cu species during electrolysis is reversible. Indeed, application of a positive potential (1.0 V *vs.* RHE) led to a complete disappearance of the Cu-Cu signal and the full restoration of the CuN_4 peak in the FT-EXAFS spectrum as well as the return of the threshold energy of the XANES spectrum to that characteristic of Cu^{2+} (Figure 4b). It is interesting to point out that the typical pre-edge feature at 8986 eV clearly visible in the pre-electrolysis XANES spectrum of CuPolyPc@CNT, is damped in the post-electrolysis XANES spectrum. This peak has been assigned to a shake-down 1s → 4pz transition characteristic for a square-planar configuration with high D4h symmetry[9], so its reduction is an indication of a molecular distortion involving the plane containing the CuN4 sites.

Conclusion

We have reported here an original Cu-based catalytic hybrid material, consisting of a polymer of Cu phtalocyanine coated on carbon nanotubes (CNTs), for CO_2 electroreduction to CO. The synthesis, via *in situ* polymerization on CNTs using cheap organic precursors and Cu salt, is straightforward and the material only displays isolated Cu sites, within a phtalocyanine-like CuN_4 coordination, as shown by spectroscopy and electron microscopy methods. As a catalyst, this hybrid material proved selective for CO production (Faradic yield 80%) at relatively low overpotentials, greatly surpassing molecular Cu phtalocyanine under similar conditions, and demonstrated high robustness, as stable current and selectivity were achieved during 50 hours electrolysis.

There is only one precedent of this class of hybrid catalyst for CO_2 electroreduction, namely a previously reported CoPolyPc@CNT material displaying comparable performances[5]. It should be noted that the positive effect of the polymerization on activity and selectivity is much greater in the case of Cu-phtalocyanine than in the case of Co-phtalocyanine. When compared to other previously reported Cu-based materials with CuN_4 sites or with Cu particles on N-doped graphene, the CuPolyPc@CNT hybrid material was by far the most selective for CO production (Table S1). Remarkably, this is achieved with the highest current densities and the lowest potentials of the series shown in Table S2. Further studies are required to understand this unique selectivity. However this is particularly difficult since in this particular case the material is a precursor of the catalytic species and furthermore the latter form transiently during electrolysis.

Furthermore, we demonstrate for the first time with this class of catalyst that an extensive restructuration of the metal sites occur under operation at cathodic potentials since the Cu atoms are converted into Cu nanoparticles, which are likely to be the catalytic species. On the other hand, the particles derived from the CuPolyPc@CNT hybrid material are clearly different from those derived from molecular CuPc, since the former promote CO formation while the latter promote CH_4 formation[2j]. While intriguing, this is likely due to differences in the nature of both the Cu precursor and the support used in the two systems.

Our observations raise the question whether such a restructuration is a general feature of this class of hybrid catalysts. Furthermore, the material has the remarkable property to return to its initial state, with only isolated CuN_4 sites, after reoxidation, likely due to the strong Cu(II)-chelating capacity of the N4 sites of the material. This tells that post-characterization of this kind of materials is not sufficient to assign the catalytic activity to the isolated metal sites and that *operando* spectroscopic characterization is absolutely requested before a conclusion on the nature of the actual active sites can be reached.

Acknowledgements

D.K. acknowledges financial support from Fondation de l'Orangerie. We acknowledge Synchrotron SOLEIL (Gif-sur Yvette, France) for provision of synchrotron radiation facilities at beamline SAMBA (proposal number 99190060). We also acknowledge METSA microscopy French network for the STEM-EELS experiments.

Materials and Methods

Synthesis of the CuPolyPc@CNT and CuPolyPc@CNF

CuPolyPc@CNT was prepared by 2.5 hours heating 8.9 mg of 1,2,4,5-tetracyanobenzene (TCNB) together with 3.4 mg of cuprous chloride ($CuCl_2$), thus in 2:1 molar ratio, under Ar atmosphere on 20 mg multi-walled CNT templates, previously treated with acid and dispersed in ethylene glycol. The resulting product was washed then with H_2SO_4 (8 M) aqueous solution, acetone, ethanol and dried under vacuum for 12h.

Multi-walled carbon nanotubes (CNTs) and carbon nanofibers (iron-free) (CNFs) were acquired from Sigma-Aldrich. CNTs and CNFs were used after acid treatment. The raw carbon materials were dispersed in H_2SO_4 (8 M) and sonicated for 4 h and then washed repeatedly with deionized water until the pH value got close to 7. They were finally dried in a vacuum oven at 85 °C overnight.[10]

The same protocol was used for the preparation of CuPolyPc@CNF.

Preparation of Cu Phthalocyanine on CNT

For control experiments 15.1 mg copper (II) phthalocyanine (CuPc) (Sigma-Aldrich) was mixed with 20 mg of multi-walled CNT and dispersed in 5 ml of THF. The suspension was sonicated for 5 hours. Then the solvent was evaporated.

Electrode Preparation

2 mg of the catalyst was sonicated for 2 h in 400 µl of isopropyl alcohol and 5 µl of a Nafion® perfluorinated resin solution (5 wt.% in mixture of lower aliphatic alcohols and water, containing 5% water). Then, the suspension was deposited by drop-casting (one drop every 30 seconds) on a GDL (AVCarb GDS 3250) (1 cm^2) and dried in air at 100 °C for 30 minutes.

For the control experiments, the working electrodes were prepared by similar way.

Electrode characterization

TEM images were obtained on a JEM-2010F transmission electron microscope (JEOL) with an accelerating voltage of 200 kV. High angle annular dark field scanning transmission electron microscopy imaging experiments were performed in a NION UltraSTEM 200 operated at 60 keV.

X-ray photoelectron spectra (XPS) were collected using a Thermo Electron Escalab 250 spectrometer with a monochromated Al Kα radiation (1486.6 eV). The analyzer pass energy was 100 eV for survey spectra and 20 eV for high-resolution spectra. The analyzed area was 500 mm2. The photoelectron take-off angle (angle between the surface and the direction in which the photoelectrons are analyzed) was 90°. Curve fitting of the spectra was performed with the Thermo Electron software, Avantage. Cu Auger peak deconvolution was carried out using spectra of Cu phthalocyanine, Cu_2O and Cu standards measured on the same instrument as a reference for Cu^{2+}, Cu^{+} and Cu^{0} species, respectively. Shirley background correction was applied to all peaks before deconvolution.

Copper content within catalytic material was quantified with inductively coupled plasma-atomic emission spectroscopy (ICP-AES) in a Thermo Scientific iCAP 6300 duo device after digestion of the graphitic structures in a 3:1 H_2SO_4 (96% wt pure)– HNO_3 (56% wt pure) acid mixture, followed by filtration.

Electrochemical characterization

All electrochemical measurements were performed in a three-electrode two-compartment cell using a Bio-logic SP300 potentiostat, with a reference electrode, namely Ag/AgCl/3M KCl (hereafter abbreviated as Ag/AgCl), placed in the same compartment as the working electrode. A platinum counter electrode was placed in a separate compartment. The two compartments were separated by a membrane (Fumasep FBM- Bipolar Membrane). The electrolyte was CO_2-saturated 0.1 M $CsHCO_3$. The electrochemical cell was first purged with CO_2 at a flow rate of 25 mL/min during one hour prior to catalytic tests, and then, during electrolysis, continuously purged with CO_2 at a fixed flow rate using a mass flow controller (Bronkhorst EL-FLOW model F-201CV). All electrochemical data was referenced to RHE using the following equation: E(V *vs.* RHE) = E(V *vs*. Ag/AgCl.) + E(V of Ag/AgCl. *vs*. NHE) + 0.059×pH, with E(V of Ag/AgCl. *vs*. NHE) = 0.205 V and a pH value of 6.8 for the electrolyte. The effluent gas products from the electrochemical cell were identified and quantified using a gas chromatograph (SRI 8610C) equipped with a packed Molecular Sieve 5 Å column for permanent gases separation and a packed Haysep-D column for light hydrocarbons separation. Argon (Linde 5.0) was used as carrier gas. A flame ionization detector (FID) coupled to a methanizer was used to quantify CO, methane and hydrocarbons while a thermal conductivity detector (TCD) was used to quantify H_2.

Liquid phase products were quantified by ^{1}H NMR (Bruker AVANCE III 300 MHz spectrometer using a Pre-SAT180 water suppression method[11]). Samples were prepared by mixing a 300 µl aliquot of electrolyte solution with 50 µl D_2O used for NMR-locking and 10 µl of acetonitrile used as internal standard (1 µmol).

Electrochemically active surface area measurements

Electrochemically active surface areas of the different electrodes were estimated by probing the redox reaction of the ferricyanide/ferrocyanide couple using cyclic voltammetry (CV). 0.1 M KCl solution containing 10 mM ferrocyanide was initially degassed with Ar. Then the potential of the working electrode was swept between 600 mV and –200 mV *vs.* Ag/AgCl (1 M KCl) at different scan rates (mV/s). Between each CV at different rates, the solution was bubbled with Ar and shaken to quickly reach back to the initial conditions. Electrochemically active surface areas (ECSA) were estimated from the Randles-Sevcik equation, as follows: $I_p = (2.69 \times 10^5)\, n^{3/2}\, A\, D^{1/2}\, \upsilon^{1/2}\, C$, with I_p : peak current, n : number of moles of electrons per mole of electroactive species, A : area of electrode (cm^2) , D : diffusion coefficient (cm^2/s), υ : scan rate (V/s), C : concentration (mol/cm^3). The diffusion coefficient of ferricyanide is 6.7×10^{-6} cm^2 /s and its concentration 10^{-5} mol/cm^3. The ECSA (A) is estimated from the slope of the plot of I_p versus $\upsilon^{1/2}$.

***Operando* XAS experiment**

Operando XAS measurements were collected at room temperature at SAMBA beamline (Synchrotron SOLEIL) equipped with a double crystal Si 220 monochromator. For the sample preparation, 10 mg of the catalyst material was sonicated for 30 minutes in 50 µl of isopropyl alcohol and 100 µl of a Nafion® perfluorinated resin solution (5 wt.% in mixture of lower aliphatic alcohols and water, containing 5% water).Then, 50 µl of catalyst ink was drop-casted (one drop per 30 second) on a 3 cm^2 circular area of a 100-µm-thick graphite foil (Goodfellow cat. C 000200/2), resulting in a catalyst loading of ~1 mg cm^{-2} followed by a drying step in air at 100 °C for 30 minutes. The graphite foil was then used as a working electrode and was installed in an electrochemical cell (PECC2, from Zahner), as in previous experiments[12] and as shown in Figure S13. The counter electrode was a Pt wire and reference electrode was Ag/AgCl/3 M KCl. The cell was filled with aqueous 0.1M $CsHCO_3$. During the electrolysis the cell was continuously

bubbled with CO_2. *Operando* measurements were performed by recording the K_α X-ray fluorescence of Cu with a Canberra 35-elements monolithic planar Ge pixel array detector.

EXAFS data analysis

The EXAFS data analysis was carried out by using the GNXAS approach, which is based on the decomposition of the experimental EXAFS χ(k) signal into a summation over n-body distribution functions γ(n) calculated by means of the multiple-scattering (MS) theory.[13] The spectra of copper foil and CuPolyPc@CNT at -1.2V have been modelled with γ-like distribution functions which depend on four parameters: the coordination number N, the average distance R, the mean-square variation σ2, and the skewness β. Least-square fits of the EXAFS raw experimental data have been performed by minimizing a residual function of the type:

$$R_i\left(\{\lambda\}\right) = \sum_{i=1}^{N} \frac{[\alpha_{\exp(E_i)} - \alpha_{mod}(E_i\,;\,\lambda_1, \lambda_2, \ldots, \lambda_p)]^2}{\sigma_i^2}$$

where N is the number of experimental points, Ei, λi (i=1…p) are the p parameters to be refined and σ2i is the variance associated with each experimental point αexp(Ei). Additional non-structural parameters were minimized, namely E0 (core ionization threshold energy) and S02 (amplitude reduction factor) taking into account intrinsic losses.

The interpretation of the CuPolyPc@CNT spectrum collected at -1.2V was achieved on the basis of an in-depth analysis of bulk Cu, for which we used a known face-centered cubic crystal structure, then employed for refining the CuPolyPc@CNT data. For copper foil the Cu-Cu bond distances are, within the statistical errors, in perfect agreement with previous crystallographic determinations[14] then validating the reliability of the fitting procedure.

REFERENCES

[1] D. U. Nielsen, X.-M. Hu, K. Daasbjerg, T. Skrydstrup, *Nature Catalysis* **2018**, *1*, 244-254.

[2] a) S. Meshitsuka, M. Ichikawa, K. Tamaru, *Journal of the Chemical Society, Chemical Communications* **1974**, 158-159; b) C. M. Lieber, N. S. Lewis, *Journal of the American Chemical Society* **1984**, *106*, 5033-5034; c) N. Furuya, K. Matsui, *Journal of Electroanalytical Chemistry and Interfacial Electrochemistry* **1989**, *271*, 181-191; d) C. Costentin, S. Drouet, M. Robert, J. M. Saveant, *Science* **2012**, *338*, 90-94; e) G. F. Manbeck, E. Fujita, *Journal of Porphyrins and Phthalocyanines* **2015**, *19*, 45-64; f) J. Shen, R. Kortlever, R. Kas, Y. Y. Birdja, O. Diaz-Morales, Y. Kwon, I. Ledezma-Yanez, K. J. P. Schouten, G. Mul, M. T. M. Koper, *Nature Communications* **2015**, *6*, 8177; g) Z. Weng, J. Jiang, Y. Wu, Z. Wu, X. Guo, K. L. Materna, W. Liu, V. S. Batista, G. W. Brudvig, H. Wang, *Journal of the American Chemical Society* **2016**, *138*, 8076-8079; h) N. Morlanés, K. Takanabe, V. Rodionov, *ACS Catalysis* **2016**, *6*, 3092-3095; i) S. Kusama, T. Saito, H. Hashiba, A. Sakai, S. Yotsuhashi, *ACS Catalysis* **2017**, *7*, 8382-8385; j) Z. Weng, Y. Wu, M. Wang, J. Jiang, K. Yang, S. Huo, X.-F. Wang, Q. Ma, G. W. Brudvig, V. S. Batista, Y. Liang, Z. Feng, H. Wang, *Nature Communications* **2018**, *9*, 415.

[3] a) H. Zhao, Y. Zhang, B. Zhao, Y. Chang, Z. Li, *Environmental Science & Technology* **2012**, *46*, 5198-5204; b) X. Zhang, Z. Wu, X. Zhang, L. Li, Y. Li, H. Xu, X. Li, X. Yu, Z. Zhang, Y. Liang, H. Wang, *Nature Communications* **2017**, *8*, 14675; c) A. Maurin, M. Robert, *Journal of the American Chemical Society* **2016**, *138*, 2492-2495.

[4] S. Lin, C. S. Diercks, Y. B. Zhang, N. Kornienko, E. M. Nichols, Y. Zhao, A. R. Paris, D. Kim, P. Yang, O. M. Yaghi, C. J. Chang, *Science* **2015**, *349*, 1208-1213.

[5] N. Han, Y. Wang, L. Ma, J. Wen, J. Li, H. Zheng, K. Nie, X. Wang, F. Zhao, Y. Li, J. Fan, J. Zhong, T. Wu, D. J. Miller, J. Lu, S.-T. Lee, Y. Li, *Chem* **2017**, *3*, 652-664.

[6] a) M. Abel, S. Clair, O. Ourdjini, M. Mossoyan, L. Porte, *Journal of the American Chemical Society* **2011**, *133*, 1203-1205; b) X. Wang, B. Wang, J. Zhong, F. Zhao, N. Han, W. Huang, M. Zeng, J. Fan, Y. Li, *Nano Research* **2016**, *9*, 1497-1506.

[7] A. Epstein, B. S. Wildi, *The Journal of Chemical Physics* **1960**, *32*, 324-329.

[8] a) A. Murata, Y. Hori, *Bulletin of the Chemical Society of Japan* **1991**, *64*, 123-127; b) M. R. Thorson, K. I. Siil, P. J. A. Kenis, *Journal of The Electrochemical Society* **2013**, *160*, F69-F74; c) M. R. Singh, Y. Kwon, Y. Lum, J. W. Ager, A. T. Bell, *Journal of the American Chemical Society* **2016**, *138*, 13006-13012; d) J. Resasco, L. D. Chen, E. Clark, C. Tsai, C. Hahn, T. F. Jaramillo, K. Chan, A. T. Bell, *Journal of the American Chemical Society* **2017**, *139*, 11277-11287.

[9] a) T. A. Smith, J. E. Penner-Hahn, M. A. Berding, S. Doniach, K. O. Hodgson, *Journal of the American Chemical Society* **1985**, *107*, 5945-5955; b) J. L. DuBois, P. Mukherjee, T. D. P. Stack, B. Hedman, E. I. Solomon, K. O. Hodgson, *Journal of the American Chemical Society* **2000**, *122*, 5775-5787.

[10] L. Zhao, Z.-B. Wang, X.-L. Sui, G.-P. Yin, *Journal of Power Sources* **2014**, *245*, 637-643.

[11] H. Mo, D. Raftery, *Journal of magnetic resonance (San Diego, Calif. : 1997)* **2008**, *190*, 1-6.

[12] A. Zitolo, N. Ranjbar-Sahraie, T. Mineva, J. Li, Q. Jia, S. Stamatin, G. F. Harrington, S. M. Lyth, P. Krtil, S. Mukerjee, E. Fonda, F. Jaouen, *Nature Communications* **2017**, *8*, 957.

[13] a) A. Filipponi, A. Di Cicco, C. R. Natoli, *Physical Review B* **1995**, *52*, 15122-15134; b) A. Filipponi, A. Di Cicco, *Physical Review B* **1995**, *52*, 15135-15149.

[14] R. W. G. Wyckoff, *Crystal structures Vol. 1. Vol. 1*, Interscience., New York; London, **1963**.